AIAA JOURNAL
Vol. 42, No. 3, March 2004

Time-Series Analysis of Supersonic Base-Pressure Fluctuations

Jonathan R. Janssen* and J. Craig Dutton†
University of Illinois at Urbana–Champaign, Urbana, Illinois 61801

An investigation into the dynamic nature of supersonic base-pressure fluctuations was conducted. Two axisymmetric models, a blunt and a boattailed afterbody, were studied at a freestream Mach number of 2.46 and zero angle of attack. High-frequency pressure measurements were recorded with both radially and circumferentially positioned transducers. Blunt afterbody measurements showed rms pressure fluctuations on the order of 5% of the average base pressure. Power spectral density (PSD) estimates at the two outermost radial locations for the blunt afterbody revealed that a significant portion of the pressure fluctuation energy is contained in a peak centered near 850 Hz ($Sr = 0.094$). RMS pressure fluctuations on the boattailed afterbody were on the order of 4.3% of the average base pressure. The PSD estimates at the two outermost locations contained a more defined and larger peak centered near 800 Hz ($Sr = 0.089$) as compared to the blunt base. The two outermost radial locations on both afterbodies are subjected to similar pressure histories and, hence, display large values of coherence at low frequencies. The pressure history at the center position is not well correlated to those at the two outermost locations, resulting in low values of coherence. Possible mechanisms for the substantial pressure fluctuation energy contained at low frequencies are pulsing or flapping of the recirculation region, whereas higher-frequency energy could be attributed to large-scale turbulent structures in the shear layer.

Introduction

AXISYMMETRIC supersonic base flows have been studied in great detail for well over 50 years, yet understanding of the fundamental mechanisms that govern these flowfields is still incomplete. Interactions between these mechanisms determine base pressure, and consequently base drag, as well as other important quantities for aerodynamic bodies. Recent experimental studies of axisymmetric supersonic base flows have included mean surface-pressure measurements, laser-Doppler-velocimetry (LDV) mean velocity and Reynolds-stress measurements in the base region, particle-image-velocimetry measurements in the base region, and planar Mie/Rayleigh-scattering visualizations of the shear layer and developing wake.[1–8] Even though some of these measurement techniques produce instantaneous flowfield samples, they do so in a time-uncorrelated manner. Hence, they are incapable of producing time-series and spectral (i.e., frequency-dependent) information. Consequently, few quantitative data exist to examine the fluid dynamic mechanisms that influence the unsteady aspects of these flowfields.

A schematic of the mean near-wake region of a cylindrical blunt-based afterbody at zero angle of attack in a supersonic flowfield is shown in Fig. 1. As the supersonic flow separates from the base corner, it undergoes a strong expansion to the low pressure of the base region, and a free shear layer is formed. The shear layer separates the outer high-speed inviscid flow from the inner low-speed base recirculation region. Upon approach to the axis of symmetry, the free shear layer undergoes recompression, and shock waves occur as the flow is forced to turn along the axis of symmetry. A rear stagnation point (reattachment point) is formed on the axis where the local mean velocity of the flow equals zero. Downstream from the rear stagnation point, a trailing wake develops along the axis. From previous measurements,[1,2,9] it has been found that the interaction between the free shear layer and the base recirculation region controls the mass entrainment from the recirculation region into the shear layer. The amount of mass entrained from the recirculation region, in turn, determines the base pressure and, hence, the base drag.

Although detailed measurements have been made to investigate the mean flow, turbulence characteristics, and the dynamic nature of compressible free shear layers[10,11] and supersonic boundary layers,[12,13] few measurements have been made to investigate the dynamic nature of the recirculation region in a supersonic base flow. A small number of studies have attempted to characterize the base-pressure fluctuations on axisymmetric bodies. The majority of these studies, though, were conducted in subsonic freestream flow.[14–17] Only two previous studies were found in which base-pressure fluctuation measurements at supersonic freestream speeds were recorded for axisymmetric blunt-based bodies. Both Mabey[18] and Shvets[19] performed experiments on several axisymmetric blunt-based bodies, including cylindrical bodies with hemispherical forebodies. All models studied by both Mabey and Shvets were either strut- or downstream sting-supported. Consequently, measurements obtained in the base regions of these models might have been affected by disturbances in the flowfield created by the struts or stings. Shvets noted that as the Mach number was increased for a given body the rms base-pressure fluctuations normalized by the freestream dynamic pressure decreased in magnitude, which is opposite to the trend previously documented in subsonic base flows.[14,17] In addition, Shvets explored the effect of the length-to-diameter ratio of the model, observing that, as this ratio was increased, the normalized rms base-pressure fluctuations decreased in magnitude. Shvets did not present quantitative spectral results for the axisymmetric cylindrical models at supersonic freestream speeds, leaving the time-series analysis of supersonic base-pressure fluctuations largely unfinished.

Previous attempts at numerically predicting the base pressure and mean flow quantities in the near-wake region of supersonic base flows with Reynolds-averaged Navier–Stokes (RANS) methods have proved moderately successful.[20,21] The ability to predict the fluctuating properties of these flowfields, especially the turbulent stresses, using RANS techniques, on the other hand, remains relatively poor. New time-accurate flowfield modeling techniques, such as large-eddy simulation and detached-eddy simulation, are currently being developed in order to predict the unsteady characteristics of supersonic separated flowfields.[22–24]

To aid these computational investigations and to improve the general understanding of unsteady flow mechanisms in supersonic base

Presented as Paper 2003-3468 at the AIAA 33rd Fluid Dynamic Conference, Orlando, FL, 23–26 June 2003; received 24 July 2003; revision received 24 October 2003; accepted for publication 24 October 2003.

*Graduate Research Assistant, Department of Mechanical and Industrial Engineering, 1206 West Green Street. Student Member AIAA.

†Donald Biggar Willett Professor of Engineering, Department of Mechanical and Industrial Engineering, 1206 West Green Street. Associate Fellow AIAA.

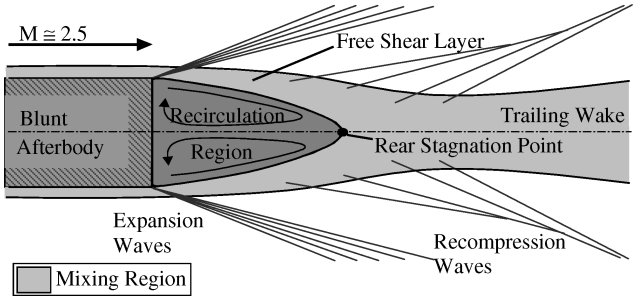

Fig. 1 Schematic of the time-averaged supersonic flow over an axisymmetric blunt afterbody.

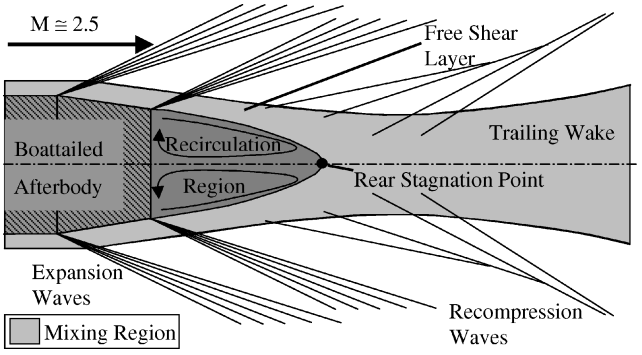

Fig. 2 Schematic of the time-averaged supersonic flow over an axisymmetric boattailed afterbody.

flows, quantitative, time-series data investigating the unsteady aspects of these flowfields must be recorded and analyzed. For this reason, the current work is directed at obtaining and analyzing time-series base-pressure measurements for a blunt and a boattailed afterbody in an axisymmetric supersonic flowfield. These measurements will help in determining the flowfield mechanisms that influence the fluctuating and time-mean pressure field in supersonic base flows.

Experimental Facilities and Procedures

All experiments described herein were conducted in the University of Illinois Gas Dynamics Laboratory. The facilities there are specifically designed for experimental studies of axisymmetric base flows at supersonic velocities. The particular experiment described in this paper was conducted using a blowdown supersonic axisymmetric wind tunnel. This wind tunnel consists of a stagnation chamber, an annular converging-diverging (c-d) nozzle, a constant-area test section viewing the base region, and a diffuser designed to aid in pressure recovery. This facility was operated at a stagnation pressure of 499.2 ± 2.1 kPa and a stagnation temperature of 294.5 ± 0.3 K, which generates a freestream Mach number of 2.46, a unit Reynolds number of 52×10^6 m^{-1}, and a freestream turbulence intensity that is less than 1% in the freestream preceding separation at the base.

Passing through the center of the c-d nozzle is a hollow, cylindrical sting. The sting is aligned on the centerline of the c-d nozzle and is supported far upstream of the nozzle, before the flow-conditioning screens and honeycomb, to prevent support interference effects in the downstream flowfield. The blunt-based afterbody has a nominal 63.5-mm diam and is attached to the downstream end of the sting using internal threads. Several ports on the base of the blunt afterbody were machined to accept a variety of plugs. The plugs are of three kinds: plug type 1 is solid such that when inserted it produces a smooth base; plug type 2 was machined such that a high-frequency pressure transducer could be inserted into it and mounted flush and normal to the base; plug type 3 is a solid plug with a static pressure port machined through the plug.

The boattailed afterbody also has a nominal 63.5-mm diam upstream of the boattail and likewise attaches to the sting by a series of internal threads. The boattail, which is a commonly used technique to increase mean base pressure, converges toward the axis at an angle of 5 deg relative to the horizontal for an axial distance of 31.75 mm. Thus, the diameter of the boattailed base at flow separation is 57.91 mm. Similar modifications to the boattailed afterbody as described for the blunt base were completed to allow mounting of the high-frequency pressure transducers. A schematic of the time-averaged supersonic flowfield near the boattailed afterbody at zero angle of attack is shown in Fig. 2. As can be seen, the primary difference between the blunt and boattailed afterbody flowfields is an additional centered expansion that occurs at the cylindrical body–boattail junction. Both afterbodies were aligned axisymmetrically with the c-d nozzle, which was confirmed by performing oil-streak visualizations on the base in the recirculation region. Oil-streak visualizations in this region have previously been found to be very sensitive to misalignment between the sting and the nozzle centerline,[1] and thus are good indicators of axisymmetric flow conditions.

Mean static-pressure measurements were obtained using a Pressure Systems, Inc., Netscanner Model 98RK. The Netscanner system contains eight Model 9816 modules, seven with pressure-sensing capability from ±0-103 kPa and one with pressure-sensing capability from ±0-689 kPa. Each module is capable of reading and recording up to 16 pressures at approximately 6 Hz. Static-pressure measurements from this system were used primarily to verify time-averaged results from the high-frequency pressure transducers because the Netscanner system is not capable of high-frequency pressure measurements.

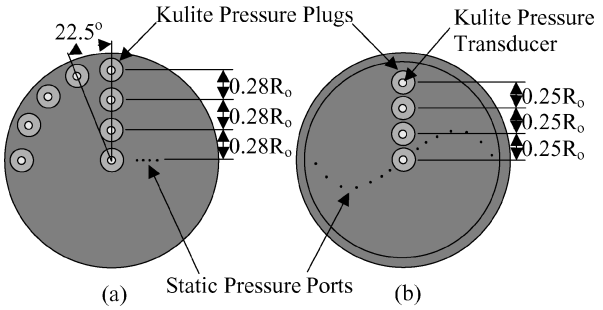

Fig. 3 Locations of various pressure measurements along a) blunt afterbody and b) boattailed afterbody.

High-frequency measurements were made with Kulite pressure transducers. Two Kulite XCS-062 pressure transducers, with a pressure sensor diameter of 0.71 mm and a pressure range of 0 to 68.95 kPa, were rigidly mounted into two plugs (type 2 in the preceding discussion) with room temperature vulcanized rubber (RTV). The Kulite transducers used were quoted as having a combined nonlinearity and hysteresis, that is, a measurement uncertainty, of 0.25% of full scale and 0.1% repeatability. The Kulite transducers were aligned along the centerline of the plugs and flush with the outer face of the plugs using spacers before the RTV was injected and allowed to cure. The plug ports were aligned along a radius from the center of the afterbodies and, in the case of the blunt afterbody, circumferentially near the outer radius of the base (Fig. 3). The transducers were statically calibrated in situ as a check after every fourth data-acquisition run with an SI Pressure Series 6000 deadweight tester that is National Institute of Standards and Technology traceable. Calibrations were shown to remain essentially constant from day to day, as the slope typically varied by less than 0.1% and the zero point by less than 1%. As demonstrated by previous authors, static calibration of these transducers is accurate to within a few percent of the dynamic values.[25] The transducers were powered by two Vishay Model 2311 signal conditioners. Output from the transducers was amplified by the signal conditioners before passing through a 16-bit National Instruments Model 6035E or Model 6036E A/D card. The two National Instruments cards were linked together via an RTSI bus cable to provide simultaneous sampling of the two transducers. The signal-to-noise ratio typical of this system was of the order of 100.

Measurements were obtained in 24-s intervals at a sampling rate of 166,667 samples/s, thereby accumulating 4,000,000 samples per run. This sampling rate was conservatively selected based on a minimum sampling rate of 1.2 to 1.3 times the Nyquist frequency, as

suggested by Bendat and Piersol.[26] The time-series data were then digitally low-pass filtered using a 20-pole Butterworth filter. A cutoff frequency of 50 kHz was selected in order to suppress the resonance frequency that occurs between the transducer diaphragm and its protective screen; this resonance frequency occurs at approximately 60 kHz for the transducers used in this experiment. Data sets of 8192 samples were analyzed using standard time-series analysis techniques,[26] as described next.

To exclude known sources of high-frequency pressure transducer measurement errors, two separate investigations were completed: a no-flow study and a stagnation chamber study. Two-transducer results under no-flow conditions showed insignificant levels of cross correlation and coherence, so that electrical noise was not a significant problem. Likewise, cross-correlation levels between the stagnation chamber and the base were negligible, so that the base-pressure fluctuations do not originate from the facility control valve.

Analysis Techniques

After computation of the mean, rms, and probability density function (PDF) results, the data sets were reduced by a Cooley–Tukey fast Fourier transform (FFT) algorithm. Before the FFT computations, data sets were modified via two data-grooming operations to improve the results of the power-spectral-density (PSD) estimates. Multiplication of a Hanning window[26] with the data sets was completed to suppress side-lobe leakage of the FFT, before the FFT calculations. In addition, the data segments were overlapped by 50% in order to reduce the increased normalized random error caused by applying the Hanning window. Frequency resolution of the PSD estimates at the sampling rate and data set size discussed above is 20.3 Hz. Additionally, the random error estimate, which is improved by the use of overlapping segments, was determined to be 4.7%. Cross correlations were computed using full zero-padding data preparation in order to estimate the cross-correlation value over the entire data segment duration. As suggested by Bendat and Piersol,[26] the two data-grooming operations just described were not employed when computing the FFTs for the coherence or cross-correlation estimates because side lobe leakage is not an issue with these analyses.

Experimental Results

The investigation into base-pressure fluctuations was performed at four different radial locations along both the blunt and boattailed afterbodies and at five different circumferential locations along the blunt afterbody, as depicted in Fig. 3. A discussion of results for the blunt afterbody will be given first, with the discussion of the boattailed results to follow.

Blunt Afterbody

High-frequency pressure measurements at four radial locations along the blunt afterbody were first time averaged and then compared both to current mean static-pressure tap measurements and to previous mean static base-pressure measurements recorded by Herrin and Dutton[1] (Fig. 4). In Fig. 4, the base pressure P_b is normalized by the freestream static pressure P_{fs}. Both the current static tap and mean high-frequency pressure measurements show similar, slight increases in base pressure with radial position as noted previously by Herrin and Dutton. The mean measurements obtained in the current investigation by both the Kulite transducers and static-pressure taps are slightly higher, by about 2%, at the radial location $r/R_o = 0.28$. The time-averaged pressure given by the Kulite transducer was also slightly higher, again by about 2%, at the outermost location. The error bars (smaller than the square Kulite data symbols in this figure) are representative of a plus or minus one-standard-deviation repeatability of the collected data. Time-averaged circumferential results are not shown here, but demonstrate a small variation of approximately 0.25% at the five circumferential locations. This is a good indication that the sting was centered and the flowfield was indeed axisymmetric.

RMS pressure fluctuation levels divided by the mean base pressure for the blunt afterbody are shown in Fig. 5. These results show

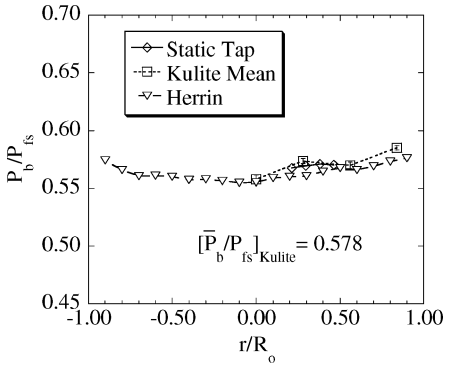

Fig. 4 Time-averaged radial base-pressure distribution for the blunt afterbody.

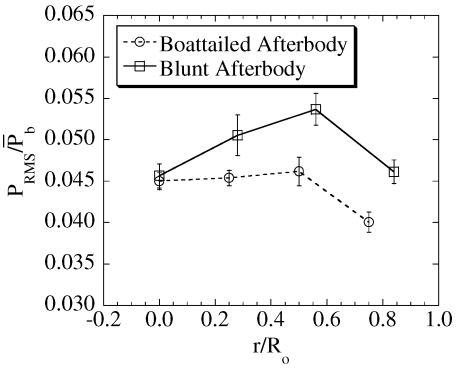

Fig. 5 Radial rms pressure distribution for the blunt and boattailed afterbodies.

that the rms pressure fluctuations are typically 5% of the mean base pressure. Similar to the time-averaged base-pressure distribution, P_b, a gradual increase in rms levels with radial location is observed, until the outermost radial location $r/R_o = 0.84$ is reached. A considerable decrease in the rms level occurs at the outermost radial location, resulting in an rms level nearly identical to the rms level at the center location. The radial rms levels differ by nearly 15% from the highest value, occurring at $r/R_o = 0.56$, to the lowest value, occurring at the base center. Again the error bars are representative of a plus or minus one-standard deviation in the collected data, that is, run-to-run variation. As with the time-averaged base-pressure results, the rms pressure fluctuation measurements at varying circumferential locations displayed a much smaller variation of approximately 2.7% over the range of circumferential positions examined.

A comparison of rms fluctuation levels from this experiment, performed on the blunt afterbody at location $r/R_o = 0.56$, and those of Shvets[19] as a function of freestream Mach number is shown in Fig. 6. In this figure, the rms pressure fluctuations are normalized with respect to the freestream dynamic pressure q_{fs}. Shvets used a strut-supported cylindrical model with a base diameter of 60 mm and a high-frequency transducer located at $r = 15$ mm, corresponding to $r/R_o = 0.50$. Performing supersonic base flow experiments at freestream Mach numbers of 1.4 and 3.0, Shvets recorded pressure–time histories and calculated the rms pressure fluctuations. The current rms measurement, obtained at a freestream Mach number of 2.46, is consistent with those of Shvets's previous findings. A decrease in rms base-pressure fluctuations normalized by the freestream dynamic pressure is noticed as the freestream Mach number is increased over the range examined.

A comparison of the PSD results at varying radial locations for the blunt afterbody is presented in Fig. 7. In this figure, $G_{pp}(f)$, the one-sided PSD as a function of frequency f, is multiplied by f and plotted on a semilog scale vs f. The PSD is plotted in this manner so that the fluctuating energy content at the corresponding frequencies is more clearly visible. Clearly, the PSDs at the two innermost radial locations and the two outermost radial locations

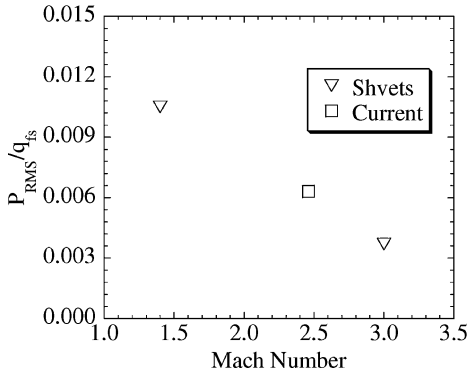

Fig. 6 RMS pressure for blunt afterbody at various freestream Mach numbers.

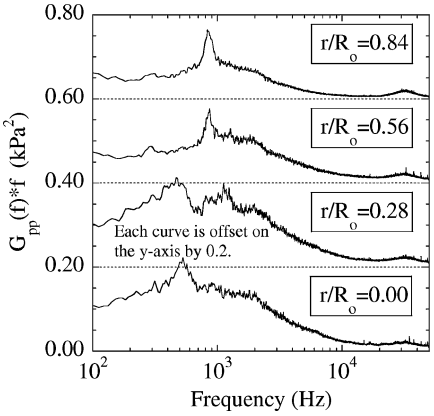

Fig. 7 One-sided PSD times frequency at various radial positions for the blunt afterbody.

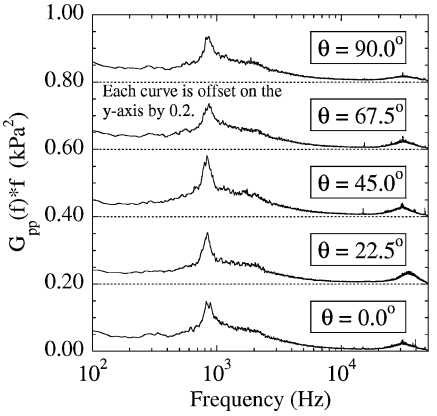

Fig. 8 One-sided PSD times frequency at various circumferential positions for the blunt afterbody.

are quite similar, with small differences between the two sets. At the two innermost radial locations, a gradual increase in the PSDs with frequency is realized until reaching peak values near 500 Hz. After the first major peaks, the PSDs at both inner locations experience similar declines until roughly 700 Hz. It is at this frequency where the PSDs for the two innermost radial locations begin to differ. Whereas at the center location $r/R_o = 0.00$, the PSD decreases slightly until about 2000 Hz; the PSD at the $r/R_o = 0.28$ location exhibits another steady increase before reaching a second peak at approximately 1200 Hz. Following this second peak, another abrupt decline occurs until roughly 1300 Hz. After 1300 Hz, the PSD at $r/R_o = 0.28$ decreases slightly, which compares well with the trend of the PSD at the center location. In the vicinity of 2000 Hz, the PSDs at both inner locations begin to decline at approximately the same rate. Frequencies above 10,000 Hz show little fluctuation energy, as the PSDs are generally small in magnitude and broadband. However, a very weak peak in the PSDs does occur in the high-frequency range at approximately 30–40 kHz.

The two outermost radial locations reveal nearly identical moderate increases in the PSD estimates for increasing frequencies up to about 700 Hz. The magnitudes of the PSDs are, however, significantly lower than those for the innermost locations at these low frequencies. Upon passing 700 Hz, the PSDs for the two outermost locations both show similar dramatic increases to nearly identical peaks near 850 Hz. The peaks for the two outermost positions are the most significant peaks in the PSD, containing on the order of 10% of the pressure fluctuations over the frequency range examined. These peaks correspond to a nondimensional Strouhal number ($Sr = fD/V$) of 0.094 based on the base diameter and the freestream velocity upstream of separation. Following these peaks, the PSDs experience sharp declines. The PSD at the outermost location $r/R_o = 0.84$ declines to a lower magnitude before leveling out around 1000 Hz than does the PSD at the third location $r/R_o = 0.56$. They both decrease in magnitude slightly until approximately 2000 Hz, after which they decline more rapidly but at slightly different rates. Similar to the innermost locations, the outermost locations show little fluctuating energy content above 10,000 Hz. The outermost locations also demonstrate a small increase in the PSD estimate between 30 and 40 kHz. This small peak seems most pronounced at the outermost radial location and might be caused by the interaction between the recirculation region and the large-scale structures in the free shear layer. The most important observation to be gained from Fig. 7 is that the majority of the energy contained in the pressure fluctuations occurs at low frequencies, that is, below a few kilohertz. The concentration of pressure-fluctuation energy at low frequencies has been noted in other supersonic separated flowfields, particularly in investigations of the separation region occurring near a compression ramp.[27] Although these two flows are subjected to different separation processes, an expansion fan for the base vs a compression shock for the ramp, the two flowfields can experience similar pressure fluctuations because of turbulent structures propagating in the free shear layers or similar motions of the separated region.

PSD results for the blunt afterbody at varying circumferential positions from 0 to 90 deg are presented in Fig. 8. The PSD estimates are nearly identical at all circumferential locations over the entire frequency range studied. These results are comparable to the already discussed PSD estimate in Fig. 7 at the outermost radial location $r/R_o = 0.84$. Additionally, because the area under the $G_{pp}(f)$ curve is equivalent to the rms pressure these circumferential PSD estimates reveal the nearly identical rms pressures at all circumferential locations studied. Finally, these results further confirm that the blunt afterbody was indeed axisymmetrically aligned within the c-d nozzle. As a result of these measurements, circumferential high-frequency pressure measurements were not deemed necessary for the boattail investigation.

The PDFs of the fluctuating base pressure were calculated for the four radial locations examined. In Fig. 9, the PDFs are plotted next to time-history samples, where time = 0 is an arbitrary point in the time series, at the corresponding radial locations for the blunt afterbody. As the radial location is increased, two major shifts in the PDFs occur. First, a general widening of the PDF is noticed with increasing radial distance until the outermost location is reached. This widening leads to an overall decrease in the peak PDF value and an increase in the rms pressure. The other major shift is a steady flattening of the slope on the high-pressure side of the PDF with increasing radial location. At the center location, the slopes of the high- and low-pressure sides of the PDF are fairly similar, with the exception of the tail that develops on the high-pressure side. As radial location increases, however, the high-pressure side slope begins to flatten, increasing the time-averaged pressure while decreasing the skewness coefficient. Kurtosis calculations also reveal a decrease in value as radial distance is increased. Consequently, the base-pressure PDF tends toward Gaussian (skewness = 0.0 and kurtosis = 3.0) as radial distance is increased. However, even at the outermost radial position, the PDF remains fairly one sided. These phenomena can also be viewed in the sample time series provided.

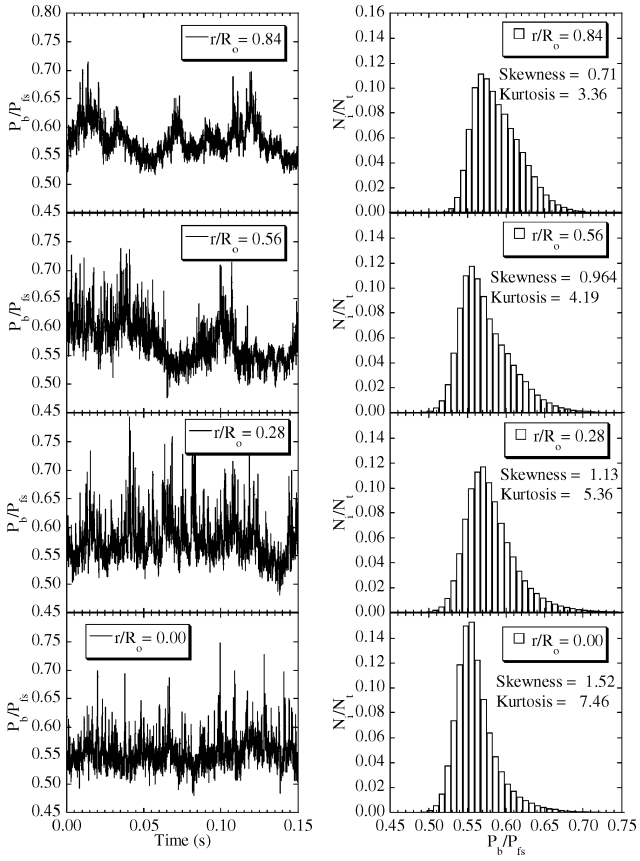

Fig. 9 Sample time-series and PDFs at various radial positions for the blunt afterbody.

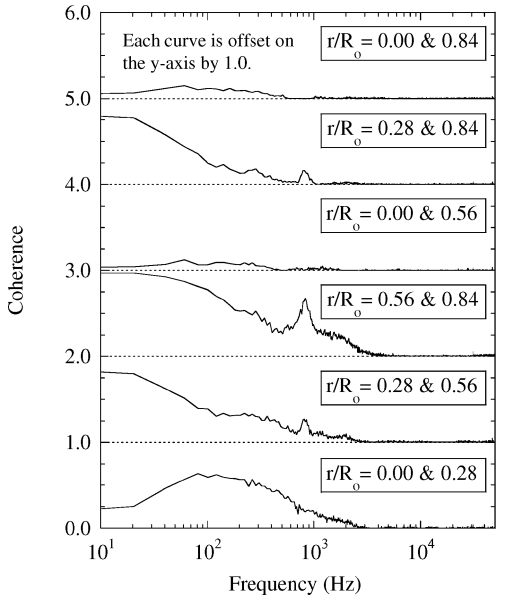

Fig. 10 Coherence coefficients at various combinations of radial positions for the blunt afterbody.

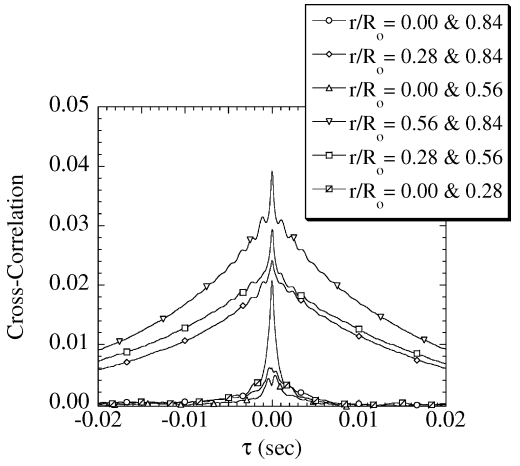

Fig. 11 Cross-correlation coefficients at various combinations of radial positions for the blunt afterbody.

At the center location, relatively small fluctuations occur about the mean pressure, with brief occurrences of high-pressure fluctuations resulting in high skewness and kurtosis values. Moving outward in radial location, larger low-frequency fluctuations occur about the mean pressure while occurrences of very high-pressure fluctuations are reduced significantly. The net result of the outward radial progression of pressure time histories is a reduction in both skewness and kurtosis values.

Simultaneous dual-transducer measurements were recorded at all six possible combinations of radial transducer locations. Coherence estimates from these measurements are shown in Fig. 10. Estimates from the simultaneous measurements at the center position in combination with either of the two outermost positions ($r/R_o = 0.00$ and 0.56 or 0.84) display very low levels of coherence at all frequencies examined. On the other hand, simultaneous sampling between the two outermost radial locations ($r/R_o = 0.56$ and 0.84) demonstrates nearly complete coherence for frequencies less than 100 Hz. For frequencies greater than 100 Hz, the coherence declines rapidly until around 500 Hz, where a sharp increase occurs to a peak centered near 850 Hz. This peak correlates well with the 850 Hz peak observed in the PSD estimates shown earlier for these two locations (Fig. 7). After the peak, a rapid decline in coherence occurs. The decline continues until reaching approximately 1000 Hz, where the coherence remains at a relatively constant, yet low, level. Upon passing 2000 Hz, the coherence estimate for these locations rapidly declines to zero. Coherence between the two middle radial locations ($r/R_o = 0.28$ and 0.56) shows a pattern similar to that for the two outermost radial locations, but at a reduced magnitude. Finally, coherence between the two innermost radial locations ($r/R_o = 0.00$ and 0.28) shows a gradual increase in coherence with frequency to about 200 Hz followed by a constant decline. Beyond 3000 Hz, the coherence remains at or near zero for all frequencies analyzed.

Cross-correlation results shown in Fig. 11 demonstrate peaks at zero time delay for all combinations of positions, with the exception of the cross correlation between the innermost radial location and the two outermost radial locations ($r/R_o = 0.00$ and 0.56 or 0.84). The lack of any well-defined peaks in the cross correlation between the center and the two outermost radial locations implies that these pressure histories are not closely correlated. This reinforces results previously noted from the coherence estimates. The combination including the two outermost radial locations ($r/R_o = 0.56$ and 0.84) displays a very sharp peak at zero time delay in addition to several small secondary peaks along the cross-correlation curve. These small peaks are representative of a time delay approximately equal to 0.0011 s. Given the distance between the two transducers, 8.9 mm, this time delay translates to a convection velocity of the pressure disturbance of 8.1 m/s, which is equivalent to a Mach number of roughly 0.02. This corresponds reasonably well to previous LDV results of Herrin and Dutton,[1] who measured a Mach number approximately equal to 0.03 for the radial flow near the outer edge of the base. Thus, a possible cause for this pressure fluctuation could be turbulent structures convecting in the low-speed boundary layer developing on the base. The fact that two time delays, a dominant one at zero time delay and a secondary one at 0.0011 s, are superimposed on one another suggests that there are at least two mechanisms contributing to the base-pressure fluctuations. Also, because the zero time delay is realized by nearly all combinations of transducer positions, a possible cause of these pressure fluctuations could be a global mechanism such as shear-layer "flapping" or "pulsing" of the recirculation region. These global mechanisms can affect the

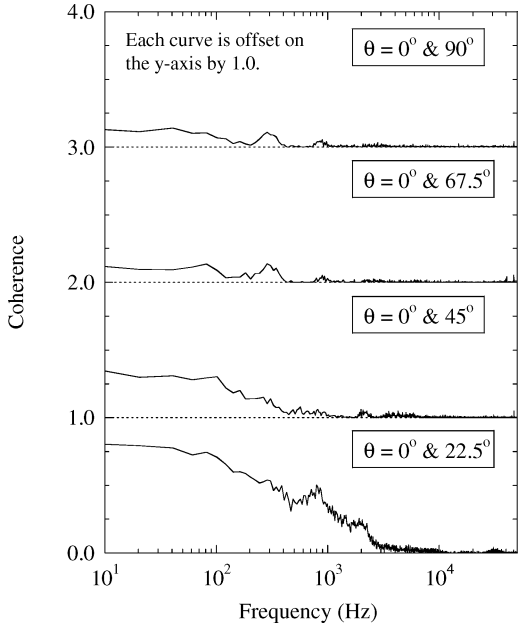

Fig. 12 Coherence coefficients at various combinations of circumferential positions for the blunt afterbody.

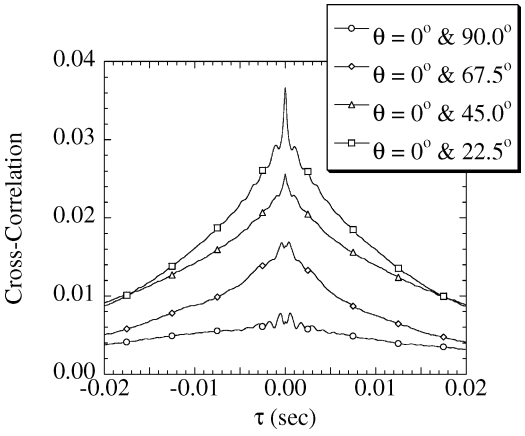

Fig. 13 Cross-correlation coefficients at various combinations of circumferential positions for the blunt afterbody.

base pressure in such a way that the resulting disturbance affects all positions on the base essentially simultaneously.

Simultaneous dual-transducer measurements recorded at varying combinations of circumferential positions at $r/R_o = 0.84$ near the outer base periphery are quantified by the coherence function and cross-correlation estimates in Figs. 12 and 13, respectively. The coherence function illustrates relatively high levels of coherence at frequencies less than 1000 Hz for adjacent circumferential positions ($r/R_o = 0.0$ and 22.5 deg). As the angle between the circumferential positions is increased, the coherence function drops in magnitude. At circumferential positions separated by more than 45 deg, the coherence function is nearly zero for all frequencies analyzed. Thus, the pressure–time histories at circumferential positions larger than 45 deg are statistically independent.

Similar results are demonstrated in the cross-correlation plot, Fig. 13. Adjacent circumferential positions show a sharp peak at zero time delay. As circumferential spacing is increased, the peak remains at zero time delay but decreases in magnitude. At the largest circumferential spacing, the cross correlation demonstrates a very slight oscillation near zero time delay and then begins to decline slowly toward zero as the time delay increases. This suggests that even at this large circumferential spacing the pressure histories are ever so slightly related. Similar to the radial case, the cross correlation between adjacent circumferential positions displays secondary peaks. Perhaps the pressure disturbances that convect with the base flow near the outer radius are large enough spatially to be experienced simultaneously by two transducers separated by 22.5 deg, but not 45 deg or greater. These secondary peaks, however, quickly dampen out as the circumferential spacing is increased.

Boattailed Afterbody

Time-averaged base-pressure results from the high-speed transducer measurements for the boattailed afterbody show even better correlation with the current and the previous static-pressure tap measurements than for the blunt afterbody (Fig. 14). These measurements also show a slight increase in base pressure with increasing radial distance, analogous to the blunt afterbody. The boattailed afterbody time-averaged base pressure is nearly 8.5% higher than for the blunt afterbody. This measured increase in average base pressure is lower than the 16% increase measured by Herrin and Dutton[2]; however, this discrepancy can be accounted for by the coarse spatial resolution in the current pressure measurements, especially at the outer radius of the afterbodies where the pressures are the highest. Because the average base pressure is an area-averaged function and the outermost radial measurement accounts for close to 50% of the area, measurements at the outermost locations dominate the results.

In addition to an increased mean base pressure, the normalized rms pressure, shown in Fig. 5, demonstrates a similar qualitative trend with radial location as for the blunt afterbody. Measurements on the boattailed base show a slight increase in rms pressure with radial distance until the outermost location where the rms pressure drops significantly. Additionally, the dimensionless rms pressure is lower for the boattailed afterbody at every radial location except for the center location where the two are nearly equal. The average rms pressure for the blunt afterbody is near 5.0% of the mean base pressure compared to the average rms pressure for the boattailed case, which is near 4.3%. Lower overall rms pressure fluctuations for the boattailed afterbody should be expected based on previous findings by Herrin and Dutton[2] and Bourdon and Dutton[6] that shear-layer growth, and thus mass entrainment, are reduced. Reduced shear-layer growth implies less mixing between the recirculation region and shear-layer fluid. Consequently, higher time-averaged base pressures and lower rms pressures are recorded for the boattailed afterbody as compared to the blunt afterbody. The reduction in rms levels might also be caused by a reduction in recirculation-region area fluctuations (pulsing) or reduced motions of the instantaneous end-view centroid of the recirculation region. Both of these phenomena were observed by Bourdon and Dutton[7] to be reduced at nearly all locations in the near-wake region for the boattailed case. A comparison of visualizations by Bourdon and Dutton of shear-layer flapping, normalized by the average shear-layer thickness, between the blunt and boattailed bases, on the other hand, was found to be equivalent or increase at all locations with the addition of a boattail. Hence, it seems that shear-layer flapping might not affect base-pressure fluctuations to a substantial degree as flapping increased while base-pressure fluctuations decreased for the boattail.

The PSDs for the four radial locations on the boattailed afterbody are shown in Fig. 15. This figure displays trends comparable

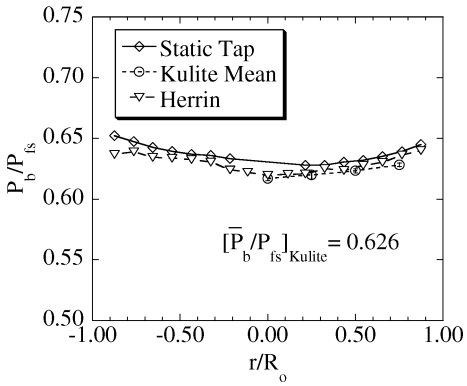

Fig. 14 Time-averaged radial base-pressure distribution for the boattailed afterbody.

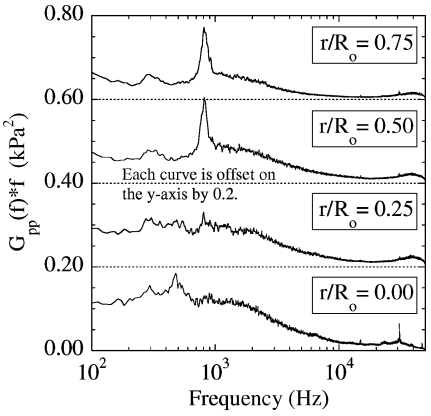

Fig. 15 One-sided PSD times frequency at various radial positions for the boattailed afterbody.

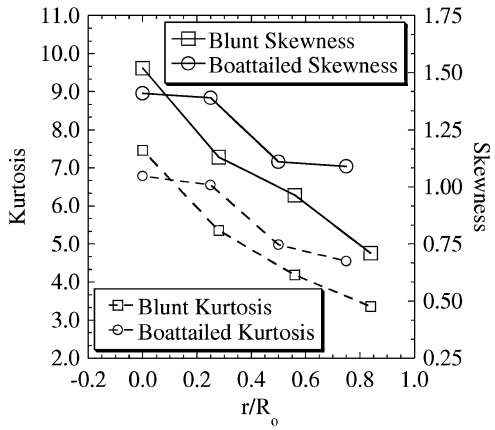

Fig. 16 Skewness and kurtosis at varying radial positions for the blunt and boattailed afterbodies.

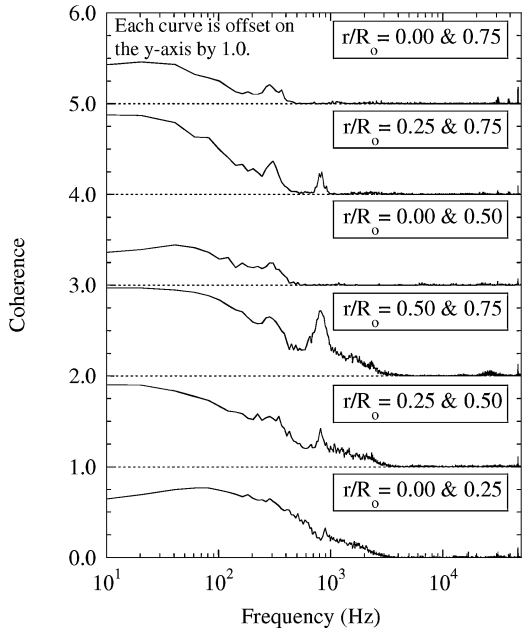

Fig. 17 Coherence coefficients at various combinations of radial positions for the boattailed afterbody.

to the blunt afterbody radial PSDs discussed earlier. The two innermost radial locations, $r/R_o = 0.00$ and 0.25, are comparable in that neither shows a significant concentration of energy at any discrete frequency. The PSD at the center location, $r/R_o = 0.00$, displays a gradual increase in energy until reaching a relatively small peak near 450 Hz. Upon reaching this small peak, the energy content decreases rapidly until 700 Hz after which the PSD remains relatively constant. At 1900 Hz the PSD begins to decrease at a relatively constant rate until 10,000 Hz, where the energy content is small. The PSD at the second radial location, $r/R_o = 0.25$, remains relatively constant with a few small peaks, of which the most notable occurs at 800 Hz, until reaching a frequency of 2000 Hz. After reaching this frequency, the energy content begins to decline at a rate similar to that of the center location. In a like manner to the center radial location, the second innermost radial location shows little energy content above 10,000 Hz.

The two outermost radial locations again display similar PSD estimates. These PSDs demonstrate one large peak near 800 Hz and a smaller peak at about 300 Hz. The large peaks realized by the two outermost positions correspond to a nondimensional Strouhal number of 0.089 based on the sting diameter before the boattail and the freestream velocity upstream of the boattail. After reaching the distinct peak near 800 Hz, the PSDs decline rapidly until about 1000 Hz. Proceeding past 1000 Hz, the PSDs show very similar results to the other two radial locations, that is, little change until passing approximately 2000 Hz, where a steady decline initiates until nearly 10,000 Hz. Additionally, a very small peak occurs in the PSDs near 40 kHz, which is most noticeable at the outer radial locations. This result is consistent with that for the blunt-base afterbody and might be related to the interaction between large turbulent structures in the shear layer and the recirculation region. With the exception of the peaks near 40 kHz, the PSDs at frequencies higher than 10,000 Hz show little energy content. Although the two PSD estimates at the outermost radial locations appear nearly identical in shape, the differences in their magnitudes are significant. The PSD at the outermost location is clearly smaller at all frequencies, but especially at frequencies greater than 1000 Hz. This difference in PSD magnitude is consistent with the smaller rms value at the outermost radial location.

Skewness and kurtosis are plotted for all four radial positions along the base of both the blunt afterbody and boattailed afterbody in Fig. 16. The boattail PDF results are comparable to those for the blunt afterbody in that a noticeable tail on the high side of the PDFs is quantitatively represented by positive skewness values. In comparison with the blunt afterbody, it is noticed that the center location for the boattailed case has noticeably lower values of skewness and kurtosis. This suggests that the pressure history at the center location of the boattailed afterbody is somewhat more Gaussian and is subjected to fewer occurrences of high-pressure fluctuations. As radial distance is increased, however, the trend reverses itself, and the boattailed afterbody reveals larger values of skewness and kurtosis when compared to the blunt afterbody results. This phenomenon might be partly caused by the fact that the dimensionless pressure transducer locations are not equal for the two afterbodies. On the other hand, even when comparing the $r/R_o = 0.56$ position of the blunt afterbody to the $r/R_o = 0.75$ position of the boattailed afterbody, higher skewness and kurtosis values occur for the boattailed afterbody. This comparison clearly shows a more dramatic change in the pressure history along the base of the blunt afterbody as compared to that for the boattailed afterbody. The cause of this difference in radial pressure history is not yet known, but it could be related to the stronger expansion/lower base pressure occurring at separation for the blunt afterbody.

The coherence results, presented in Fig. 17 for the boattailed case, are qualitatively similar to those for the blunt base. As with the blunt case, the boattailed afterbody demonstrates only low levels of coherence between simultaneous measurements at the center location and the two outermost locations ($r/R_o = 0.00$ and 0.50 or 0.75). However, the low-frequency coherence for the boattailed case is significantly larger than for the blunt case at these locations. Simultaneous measurements of the two outermost radial locations ($r/R_o = 0.50$ and 0.75) once again reveal nearly complete coherence for frequencies less than 100 Hz. Between 100 and 1000 Hz, the coherence plot for the two outermost radial locations first declines and then reveals large increases that correspond to the peaks at 300 and 800 Hz in the PSDs (Fig. 15). These trends are nearly

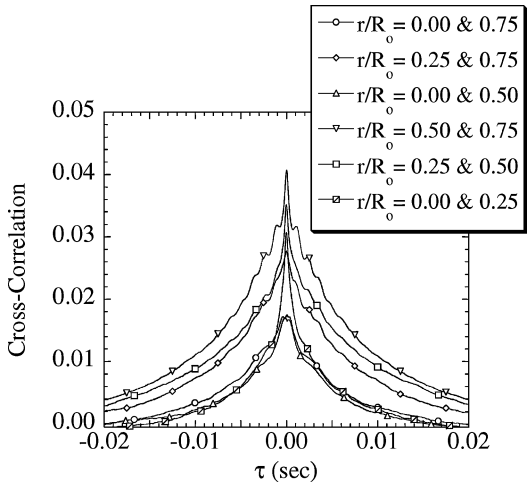

Fig. 18 Cross-correlation coefficients at various combinations of radial positions for the boattailed afterbody.

identical to those of the blunt afterbody. The lack of coherence between the center location and the outer locations lends credence to the notion of a different pressure history for the center location. Although the center location might indeed be exposed to a different pressure history than the outer locations, the second inner location, $r/R_o = 0.25$, could be described as in a transition region between the center and outermost radial locations. The $r/R_o = 0.25$ radial location demonstrates modest coherence with both the center location and the two outermost locations at various frequencies.

Finally, the cross correlations for all possible combinations of transducer radial positions along the boattailed afterbody are displayed in Fig. 18. These results again correspond well in a qualitative sense to those for the blunt afterbody. They show a peak cross correlation at zero time delay between the pressure histories at all radial transducer position combinations. For the boattailed afterbody, the cross correlation between the center location and the other three radial locations displays a more distinct peak centered on zero time delay than for the blunt case. This difference could be attributed to the reduction in the distance between the transducer locations on the boattailed afterbody in combination with the less severe change in pressure history across the boattailed afterbody. Finally, as was seen for the blunt afterbody, the cross correlations for the boattailed afterbody at the two outermost radial locations develop secondary peaks. These peaks represent a time delay of approximately 0.0012 s, which corresponds to a convection velocity of about 6.0 m/s and a Mach number of roughly 0.02. Again this velocity corresponds reasonably well with the Mach 0.03 radial flow velocity near the outer edge of the base measured by Herrin and Dutton.[2] Thus, pressure disturbances could be convected with this low-speed flow along the base.

Conclusions

Single- and dual-transducer high-frequency pressure measurements have been made at various radial locations on the base of an axisymmetric blunt and boattailed afterbody at zero angle of attack in a Mach 2.46 flowfield. High-frequency pressure measurements were also obtained at various circumferential spacings for the blunt afterbody. These measurements were intended to give insight into the dynamic nature of supersonic base flows and the mechanisms that cause pressure fluctuations. The pressure measurements were analyzed using standard time-series analysis techniques. Conclusions from these experiments are discussed next:

1) The mean pressure measurements from the high-speed transducers correspond well with previous and current mean static-pressure tap measurements for both afterbodies. As previously found in these earlier experiments, mean base pressure is increased with the addition of the boattail.

2) The normalized rms levels for both afterbodies show a slight increase with increasing radial distance until the outermost radial location is reached. At the outer radial location, the normalized rms pressures drop significantly for both afterbodies. The blunt afterbody, at all locations except for the center location, demonstrates significantly higher normalized rms levels than for the boattailed afterbody. RMS levels are near 5.0% of the average base pressure for the blunt afterbody and 4.3% for the boattailed afterbody.

3) In comparison with previous measurements by Shvets,[19] the dimensionless rms pressure for the blunt afterbody is significantly less than Shvets's rms value at Mach 1.4 and is slightly greater than Shvets's rms value at Mach 3.0. This result corresponds well with Shvets's previous finding of a general decrease in base-pressure fluctuations with increasing supersonic Mach number.

4) The power-spectral-density (PSD) measurements illustrate small differences between the base-pressure fluctuations at the two innermost and two outermost radial locations for both the blunt and boattailed afterbodies. The outer locations have, in general, lower PSD values at all frequencies except in the vicinity of 850 Hz for the blunt case and 800 Hz for the boattailed case, where a relatively sharp peak occurs. These peaks contain on the order of 10% of the rms pressure fluctuations for all frequencies examined. Strouhal numbers calculated for these peaks correspond to 0.094 and 0.089 for the blunt afterbody and the boattailed afterbody, respectively. The two innermost locations contain significantly more energy at frequencies less than 750 Hz. They also contain significantly more energy at frequencies greater than 1000 Hz. At frequencies above about 2000 Hz, the energy content declines sharply for all radial locations. Above 10,000 Hz, the energy content is quite small for all radial locations, except for weak peaks that occur in the 30–40-kHz range. This suggests that large-scale structures in the shear layer are not a major influence on base-pressure fluctuations (at least up to 50 kHz) except, perhaps, for frequencies near the small peaks just noted. Possible causes of the dominant low-frequency base-pressure fluctuations that have been measured are shear-layer flapping, pulsing of the recirculation region, and intermittent upstream boundary-layer thickening/thinning, which can influence the expansion at the base corner.

5) Probability-density-function calculations demonstrate a shift in the pressure fluctuation time histories across the base radius to reduced occurrences of high instantaneous base pressures with increased distance from the center (i.e., reduced skewness). The blunt afterbody demonstrates a more dramatic change in the pressure histories across the base radius, possibly because of the increased severity of expansion experienced at the base corner.

6) Dual-transducer measurements demonstrate nearly identical qualitative results for the blunt and boattailed afterbodies. Coherence and cross-correlation measurements for both afterbodies suggest that pressure fluctuations at the center location are not well correlated with those at the two outermost locations. Thus, the center location seems to be influenced by a somewhat different pressure history than the two outermost locations. The second innermost location displays modest coherence with both the center location and the outer locations, possibly because at this position the pressure history undergoes a transition as radial position is varied across the base. The outermost radial locations demonstrate large coherence values at low frequencies, signifying similar pressure histories. This similarity in the pressure histories at the outer locations can be caused by the fact that the flow is primarily radially directed in the neighborhood of these locations with no recirculating fluid impingements.

7) Multiple peaks in the PSDs and the coherence and cross-correlation results imply that more than one mechanism is responsible for base-pressure fluctuations in supersonic, separated flowfields. These mechanisms may include intermittent impingement of recirculating fluid on the base, shear-layer flapping, recirculation-region pulsing, and the afterbody boundary-layer thickening/thinning processes already discussed.

Acknowledgments

This project was sponsored by the U.S. Army Research Office under Grant DAAD19-01-1-0367 and was monitored by Thomas L. Doligalski. This support is gratefully appreciated.

References

[1]Herrin, J. L., and Dutton, J. C., "Supersonic Base Flow Experiments in the Near Wake of a Cylindrical Afterbody," *AIAA Journal*, Vol. 32, No. 1, 1994, pp. 77–83.

[2]Herrin, J. L., and Dutton, J. C., "Supersonic Near-Wake Afterbody Boattailing Effects on Axisymmetric Bodies," *Journal of Spacecraft and Rockets*, Vol. 31, No. 6, 1994, pp. 1021–1028.

[3]Herrin, J. L., and Dutton, J. C., "Effect of a Rapid Expansion on the Development of Compressible Free Shear Layers," *Physics of Fluids*, Vol. 7, No. 1, 1995, pp. 159–171.

[4]Herrin, J. L., and Dutton, J. C., "The Turbulence Structure of a Reattaching Axisymmetric Compressible Free Shear Layer," *Physics of Fluids*, Vol. 9, No. 11, 1997, pp. 3502–3512.

[5]Scarano, F., and van Oudheusden, B. W., "Planar Velocity Measurements of a Two-Dimensional Compressible Wake," *Experiments in Fluids*, Vol. 34, March 2003, pp. 430–441.

[6]Bourdon, C. J., and Dutton, J. C., "Planar Visualizations of Large-Scale Turbulent Structures in Axisymmetric Supersonic Separated Flows," *Physics of Fluids*, Vol. 11, No. 1, 1999, pp. 201–213.

[7]Bourdon, C. J., and Dutton, J. C., "Effects of Boattailing on the Turbulent Structure of a Compressible Base Flow," *Journal of Spacecraft and Rockets*, Vol. 38, No. 4, 2001, pp. 534–541.

[8]Bourdon, C. J., and Dutton, J. C., "Shear Layer Flapping and Interface Convolution in a Separated Supersonic Flow," *AIAA Journal*, Vol. 38, No. 10, 2000, pp. 1907–1915.

[9]Smith, K. M., and Dutton, J. C., "Investigation of Large-Scale Structures in Supersonic Planar Base Flow," *AIAA Journal*, Vol. 34, No. 6, 1996, pp. 1146–1152.

[10]Hayakawa, K., Smits, A. J., and Bogdonoff, S. M., "Turbulence Measurements in a Compressible Reattaching Shear Layer," *AIAA Journal*, Vol. 22, No. 7, 1984, pp. 889–895.

[11]Elliott, G. S., Samimy, M., and Reeder, M. F., "Pressure-Based Real-Time Measurements in Compressible Free Shear Layers," AIAA Paper 90-1980, Jan. 1990.

[12]Dawson, J. A., Samimy, M., and Arnette, S. A., "Effects of Expansions on a Supersonic Boundary Layer: Surface Pressure Measurements," *AIAA Journal*, Vol. 32, No. 11, 1994, pp. 2169–2177.

[13]Unalmis, O. H., and Dolling, D. S., "Decay of Fluctuating Wall-Pressure Field of Mach 5 Turbulent Boundary Layer," *AIAA Journal*, Vol. 37, No. 9, 1999, pp. 1088–1096.

[14]Merz, R. A., Page, R. H., and Przirembel, C. E. G., "Subsonic Axisymmetric Near-Wake Studies," *AIAA Journal*, Vol. 16, No. 7, 1978, pp. 656–662.

[15]Merz, R. A., "Subsonic Base Pressure Fluctuations," *AIAA Journal*, Vol. 17, No. 4, 1979, pp. 436–438.

[16]Liu, J. S. K., and Chow, W. L., "Axisymmetric Transonic Turbulent Base Pressures," *AIAA Journal*, Vol. 17, No. 4, 1979, pp. 330, 331.

[17]Eldred, K. M., "Base Pressure Fluctuations," *Journal of the Acoustical Society of America*, Vol. 33, No. 1, 1961, pp. 59–63.

[18]Mabey, D. G., "Some Measurements of Base Pressure Fluctuations at Subsonic and Supersonic Speeds," Aeronautical Research Council, CP 1204, London, Aug. 1970, pp. 1–19.

[19]Shvets, A. I., "Base Pressure Fluctuations," *Fluid Dynamics*, Vol. 14, No. 3, 1979, pp. 394–401.

[20]Sahu, J., "Numerical Computations of Supersonic Base Flow with Special Emphasis on Turbulence Modeling," *AIAA Journal*, Vol. 32, No. 7, 1994, pp. 1547–1549.

[21]Tucker, P. K., and Shyy, W., "A Numerical Analysis of Supersonic Flow over an Axisymmetric Afterbody," AIAA Paper 93-2347, June 1993.

[22]Fureby, C., Nilsson, Y., and Andersson, K., "Large Eddy Simulation of Supersonic Base Flow," AIAA Paper 99-0426, Jan. 1999.

[23]Forsythe, J. R., Hoffmann, K. A., and Squires, K. D., "Detached-Eddy Simulation with Compressibility Corrections Applied to a Supersonic Axisymmetric Base Flow," AIAA Paper 2002-0586, Jan. 2002.

[24]Sandberg, R. D., and Fasel, H. F., "A Flow Simulation Methodology for Compressible Turbulent Axisymmetric Wakes," AIAA Paper 2003-0267, Jan. 2003.

[25]Corcos, G. M., "Resolution of Pressure in Turbulence," *Journal of the Acoustical Society of America*, Vol. 35, No. 2, 1963, pp. 192–199.

[26]Bendat, J. S., and Piersol, A. G., *Random Data Analysis and Measurement Procedures*, 3rd ed., Wiley, New York, 2000.

[27]Beresh, S. J., Clemens, N. T., and Dolling, D. S., "Relationship Between Upstream Turbulent Boundary-Layer Velocity Fluctuations and Separation Shock Unsteadiness," *AIAA Journal*, Vol. 40, No. 12, 2002, pp. 2412–2422.

J. Gore
Associate Editor